Indian Journal of Pure & Applied Physics
Vol. 57, February 2019, pp. 95-100

# Evolution of microstructure and optical properties of $TiO_2$/Au nanocomposite

B B Tripathy[a,b], M Behera[a], H Rath[c], P Mallick[d]* & N C Mishra[b]

[a]Department of Physics, Silicon Institute of Technology, Patia, Bhubaneswar 751 024, India

[b]Department of Physics, Utkal University, Bhubaneswar 751 004, India

[c]Institute of Physics, Sachivalaya Marg, Bhubaneswar 751 005, India

[d]Department of Physics, North Orissa University, Takatpur, Baripada 757 003, India

*Received 15 February 2018; accepted 28 August 2018*

$TiO_2$/Au nanocomposite has been synthesized by mixing Au with milled $TiO_2$ nanopowder through wet chemical route. The effect of Au on the microstructural and optical properties of $TiO_2$ nanopowder has been studied by XRD, FESEM, UV Visible, PL and FTIR techniques. Our study indicates that Au causes the decrease of crystallite size of $TiO_2$ by accumulating on the circumference of these nanoparticles. $TiO_2$/Au nanocomposite exhibits strong spectral response in the visible range due to the surface plasmon effect. Band gap of $TiO_2$ nanopowder reduces from 3.4 eV to 3.1 eV while making composite with Au. The PL spectra showed that emission peak intensity of $TiO_2$ nanopowder decreases in the presence of Au. The reductions in band gap and electron-hole recombination in $TiO_2$/Au nanocomposite suggest that $TiO_2$/Au could be a good candidate for photocatalysis.

**Keywords:** Phase transformation, Ball milling, Titanium dioxide, Nanocomposite, SPR

## 1 Introduction

Titanium dioxide ($TiO_2$), a metal oxide semiconductor has been used in various applications like solar cells, sensors, memory devices, biomedical, water purifications, pigments, textiles and cosmetics owing to its non-toxicity, easy availability, excellent photocatalytic activity, outstanding chemical stability and high refractive index[1-5]. Usually, $TiO_2$ exists in three common polymorphs, like anatase (tetragonal, space group $I4_1/amd$), rutile (tetragonal, space group $P4_2/mnm$) and brokite (orthorhombic, space group Pcab)[6,7]. Two secondary high pressure forms, such as srilankite ($TiO_2$-II) (orthorhombic, space group Pbcn) and $TiO_2$-III (monoclinic, $P2_1/c$) have also been reported[8,9]. Anatase converts to srilankite at pressure and temperature of 4.75 GPa and 250 ºC, respectively[10]. Srilankite is the transient phase of anatase $TiO_2$ during ball milling and finally it transforms to rutile[11].

Among all the phases of $TiO_2$, rutile is the most stable form[12]. Applications of $TiO_2$ depend on its specific phase, for example; anatase phase of $TiO_2$ is generally used as photocatalyst, whereas, rutile phase is used in pigment industry. It is therefore crucial to understand the phase transformations processes and to control a particular phase for specific application.

Various factors like synthesis methods and parameters, post synthesis treatments (ion irradiation, thermal treatment etc.) are shown to control the phase transformation in $TiO_2$[13-15]. In addition, particle size also affects the phase transformation of $TiO_2$. Below the critical size of 14 nm, the anatase phase of $TiO_2$ is shown to be more stable than the rutile phase[16,17] and above this critical size, anatase can be transformed to rutile which can be achieved by annealing the sample with higher temperature. In recent years, noble metal nanoparticles (NPs) have been widely used as compared to other metallic NPs due to their distinct optical, electronic, chemical and mechanical properties. Among different noble metal NPs, gold (Au) NPs have been widely used in diverse field like biotechnology, industry, medicine etc. due to their properties such as large surface area, nontoxicity, chemical stability as well as unique optical, physicochemical& biological properties[18-20]. Further, Au NPs exhibit a distinct surface plasmon resonance (SPR) in visible range, originating from the coherent oscillation of the free conductive electrons. Due to this SPR, these nanoparticles are paying attention for solar cell and sensor[21,22]. The size and shape of the Au NPs detect their properties and colour verities[18,19,23].

Furthermore, it is reported that incorporation Au NPs into $TiO_2$ have shown to improve the photocatalytic activity of $TiO_2$ which could be due to

*Corresponding author: (E-mail: pravanjan_phy@yahoo.co.in)

surface plasmonic effect[24-26]. Debeila *et al.*[27] reported that the anatase to rutile phase transformation in $TiO_2$retards when doped with Au.

In this paper, we synthesized $TiO_2$/Au nanocomposite by wet chemical route and studied the effect of Au addition on the evolution of microstructural and optical properties of $TiO_2$.

## 2 Experimental

$TiO_2$ nanoparticles were synthesized from the commercially available anatase $TiO_2$ powder (purity 99%, Merck) using high energy planetary ball mill (model PM 400, Retsch). Tungsten carbide (WC) hardened balls of 10 mm diameter were used for milling with ball-to-powder mass ratio of 10:1. The powder was ground for 10 h in air, at atmospheric pressure and room temperature with speed of mill rotation ~ 300 rpm. Then the milled $TiO_2$ powder was dispersed in distilled water. To this dispersion, 0.5 wt% of $HAuCl_4$ solution was added with continuous stirring. During the stirring process, a drop of reducing agent (hydrazine hydrate) was added and the solution was stirred for 2 h at 50 ºC. The final solution was dried in an oven at 70 ºC for 3 h to obtain the $TiO_2$/Au nanocomposite powder.

Structural characterization of these samples was done using Bruker X-ray diffractometer (D8 Advance) with CuKα radiation and operated at 40 mA and 40 KV. The morphology of the powder samples was studied by using field emission scanning electron microscopy (FESEM) (Carl Zeiss, Germany). Optical characterization of these samples was done using Shimadzu UV-Visible spectrophotometer (UV-2450). Photoemission spectroscopy of the samples was recorded using a steady state spectrofluorimeter (FLS920-stm), Edinburgh Instruments UK. A Czerny-Turner type monochroator (focal length of 300 mm) and a photomultiplier tube (PMT) detector from Hamamatsu were used for collecting the spectra. All spectra were collected in the range of 250-800 nm using 266 nm as an excitation from Xe Arc Lamp source. FTIR spectra of the powder samples for spectroscopic analysis were recorded by NEXUS-870 in the frequency range of 400 $cm^{-1}$ to 4000 $cm^{-1}$.

## 3 Results and Discussion

### 3.1 Structural properties

#### *3.1.1 XRD studies*

Figure 1 shows the XRD pattern of 10 h milled $TiO_2$ and$TiO_2$/Au nanocomposite. As indicated from the XRD pattern, the peak at $2\theta$ = 25.3° corresponds to (101) plane of anatase phase [JCPDS 78-2486] in the 10 h milled powder. Other peaks at $2\theta$ = 27.4º, 36.09º, 41.2º and 54.3º correspond to the rutile phase [JCPDS 78-2485], and at $2\theta$ = 31.3º corresponds to srilankite phase [JCPDS 23-1446] of $TiO_2$ present in the XRD pattern of milled powder. In addition to the XRD peaks of 10 hr milled $TiO_2$, the peaks at $2\theta$ =38.4º and 44.5º correspond to (111) and (200) crystal planes of Au, respectively, [JCPDS 04-0784] present in the $TiO_2$/Au nanocomposite. The presence of Au peaks along with the peaks of $TiO_2$ confirms the formation of $TiO_2$/Au nanocomposite.

The development of srilankite and rutile phases in milled $TiO_2$ shows that milling induces phase transformation from anatase to stable phase of rutile through the intermediate high pressure srilankite phase. Similar results are also reported by many researchers[28-32]. Though 10 h milled $TiO_2$ and $TiO_2$/Au nanocomposite exhibit similar XRD patterns (relating to major phases) but there is a variation in the relative intensity of peaks due to (101) anatase phase. In $TiO_2$/Au nanocomposite, the integrated area of (101) anatase crystal plane is more as compared to milled $TiO_2$ powder, which could be due to the transformation from amorphous to crystalline anatase $TiO_2$, as the integrated peak area of (101) srilankite plane is almost unaltered. Further, it has reported that water acts as catalyst for the transformation from amorphous to anatase phase basically due to the rearrangement of covalent bonds[33]. This is facilitated by creation, migrations and recombination of dangling bond sites[34]. While$TiO_2$/Au nanocomposite is prepared by dispersing milled $TiO_2$ powder in distilled water, we therefore believe that water plays

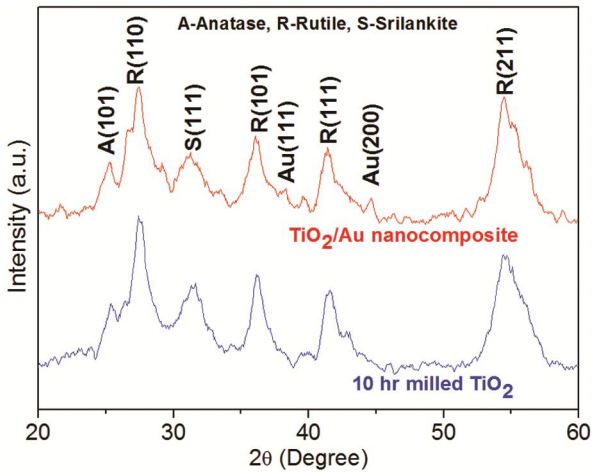


Fig. 1 – Powder XRD patterns of 10 h milled $TiO_2$ and $TiO_2$/Au nanocomposite.

the crucial role in crystallizing the amorphous to anatase$TiO_2$as reported by Yanagisawa and Ovenstone[26]. Moreover, Loganathan *et al.*[35] reported that Au has negligible influence on the crystallization of nano $TiO_2$.

The crystallite size ($D$) of the samples is calculated by Scherer formula:

$$D = \frac{0.9\lambda}{\beta cos\theta}, \quad ...(1)$$

where $\beta$ is full width at half maxima (FWHM) and $\lambda$ is wavelength of X-ray radiation. The crystallite size of the un-milled powder, having only anatase phase is 51 nm[28]. On the other hand, the crystallite size for both rutile and anatase phases of $TiO_2$/Au nanocomposite is decreased as compared to un-milled and milled $TiO_2$ powder. This decrease of crystallite size could be due to the effect of Au in $TiO_2$ matrix. The crystallite size of the rutile and anatase phases present in 10 hr milled $TiO_2$ and $TiO_2$/Au nanocomposite are given in Table 1.

#### *3.1.2 FESEM studies*

The FESEM image and EDS spectrum of $TiO_2$/Au nanocomposite are shown in Fig. 2 (a) and (b), respectively. The EDS spectrum (Fig. 2(b)), confirms the existence of Au in the $TiO_2$ matrix, as observed in XRD spectra. In case of un-milled powder, particles are almost spherical and size is about 80 nm, while in 10 h milled powder particles are irregular in shape and highly agglomerated with an average particle size of ~ 17 nm[28]. As observed in Fig. 2(a), the average particle size is ~ 14 nm. Thus, presence of Au in $TiO_2$ is not facilitating the grain growth or agglomeration of $TiO_2$ particles.

Table 1 – Crystallite size and band gap of $TiO_2$ in 10 h milled $TiO_2$ and $TiO_2$/Au nanocomposite.

| Parameters | 10 h milled $TiO_2$ | | $TiO_2$/Au nanocomposite | |
|---|---|---|---|---|
| Crystallite size, $D$ (nm) | Anatase | rutile | anatase | rutile |
| | 12.6 | 7.8 | 8.3 | 7.4 |
| Band gap (eV) | 3.34[28] | | 3.1 | |

### 3.2 Optical properties

#### *3.2.1 UV-Visible studies*

Figure 3 shows the variation of absorbance spectra of $TiO_2$/Au nanocomposite with wavelength. As indicated from the figure, $TiO_2$/Au nanocomposite exhibits a strong spectral response in the visible range (490 to 600 nm) with peak at 550 nm. The appearance of peak at 550 nm is due to surface plasmon resonance effect. The plasmon band at 550 nm can be ascribed to gold nanodots[36-38].

We calculated the size ($d$) of Au nanoparticles from the SPR peak as per the following relation[39]:

$$d = \exp\left( B_1 \frac{A_{SPR}}{A_{450}} - B_2 \right) \quad ...(2)$$

where $A_{SPR}$ and $A_{450}$ are the absorbance at SPR and 450 nm, respectively. Using the value of $\frac{A_{SPR}}{A_{450}}$ and considering the reported values[39] of $B_1$, $B_2$ as 3.55 and 3.11, respectively, we estimated the particle size of Au as 3.57 nm.

The band gap of the powder samples is calculated using the Tauc plot. In the Tauc plot energy, $h\nu$ is taken along abscissa and $(\alpha h\nu)^{1/n}$ is taken in the ordinate, where α is the absorption co-efficient, the extrapolating the linear part of Tauc plot gives the band gap energy, $E_g$. For direct transition $n$=1/2 and for indirect transition $n$=2. $TiO_2$/Au nanocomposite shows the existence of direct transition (Fig. 4) with

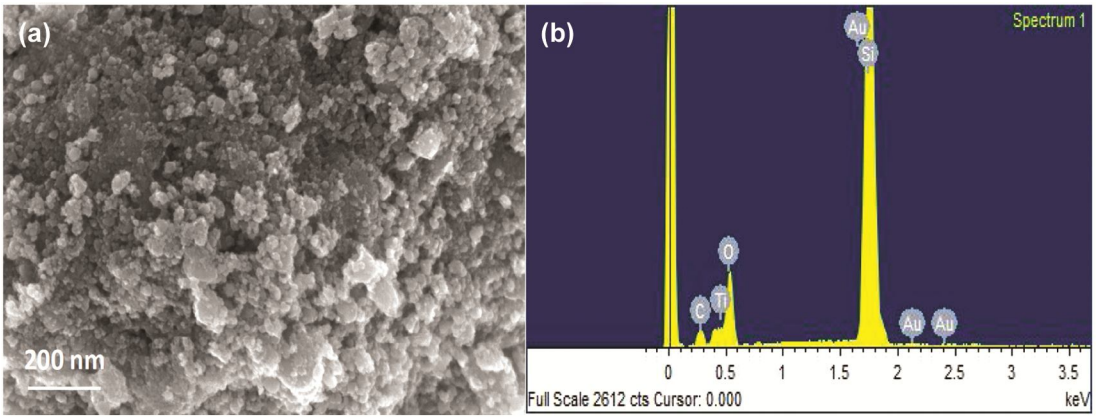


Fig. 2 – (a) FESEM images and (b) energy dispersive spectroscopy (EDS) of $TiO_2$/Au nanocomposite.

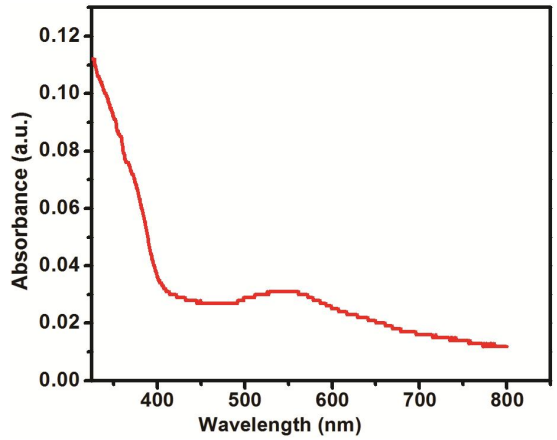


Fig. 3 – The absorbance versus wavelength for $TiO_2$/Au nanocomposite.

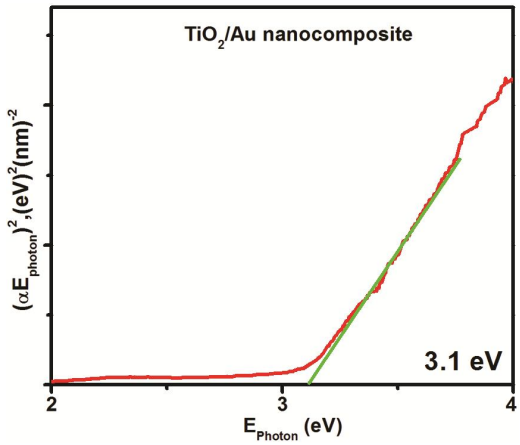


Fig. 4 – Tauc plot for $TiO_2$/Au nanocomposite.

band gap of 3.1 eV which is smaller as compared to the10 h milled $TiO_2$, *i.e.*, 3.34 eV[28]. The red shift of band gap excitation is accordance with the literature for Au incorporated $TiO_2$ nanoparticles[40]. Moreover, $TiO_2$/Au nanocomposite shows stronger light absorbance in the UV range than pure $TiO_2$. Photo excited electrons can be transferred from the conduction band of the semiconductor to the Au particles deposited on the surface of $TiO_2$ while photo generated holes remain in the valence band of $TiO_2$ as the Fermi levels of the Au are lower than that of $TiO_2$. This phenomenon greatly reduces the possibility of electron-hole recombination; hence $TiO_2$/Au nanocomposite can increase the photocatalytic activity.

### *3.2.2 PL studies*

PL emission spectra of 10 h milled $TiO_2$ and $TiO_2$/Au nanocompositeare obtained by excitation energy 266 nm and are shown in the Fig. 5. The

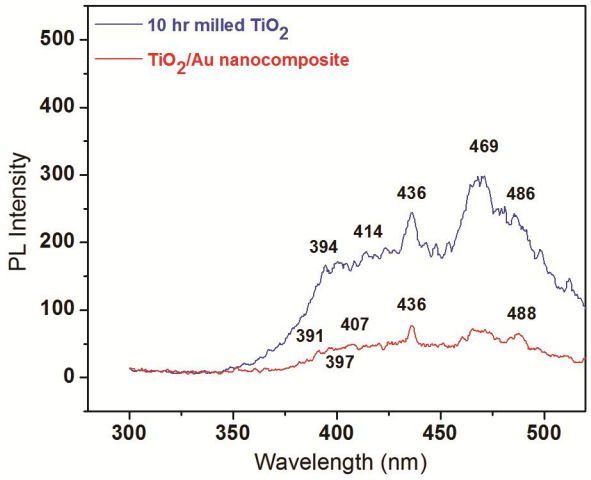


Fig. 5 – PL spectra of 10 h milled $TiO_2$ and $TiO_2$/Au nanocomposite.

emission peak at 390 nm can be ascribed to the transition of electrons from the conduction band minimum to the valence band maximum, placed at two different locations in Brillouin zone[41]. Besides 390 nm peak, all other emission peaks in the PL spectra are mainly associated with excitons and oxygen defects[42,43]. For example, the emission at 431 nm is due to self-trapped exciton of the $TiO_2$ nanoparticles[42,44] and the peak at 466 nm band is attributed to oxygen vacancies[41].

The appearance of prominent emission peaks at 435 nm and 466 nm in the PL spectra are reported for un-milled $TiO_2$[28]. The most prominent peak of un-milled $TiO_2$ (466 nm) is getting widen for 10 h milled $TiO_2$ powder primarily due to the disturbance made by strong lattice vibrations[45], which occurs during milling. The same is further widened for $TiO_2$/Au nanocomposite. The red shift in $TiO_2$/Au nanocomposite shows the band gap narrowing and is consistent with UV Visible results. The PL intensities of milled $TiO_2$ and $TiO_2$/Au nanocomposite are decreasing. This decrease in intensity is related with creation of defects and trap centres. Further, during the process of milling defects are created, which reduce electron-hole recombination. It is reported that oxygen vacancy quenches the emission intensity as it inhibits electron-hole recombination process by acting as electron trap[46]. Moreover, in case of $TiO_2$/Au nanocomposite, in addition to defects, Au nanoparticles also act as trap centres in capturing photo induced electrons, hence inhibiting electron-hole recombination and thereby decreasing peak intensity[47]. As an excellent conductor, Au metal could facilitate the rapid transfer of photoelectrons from the

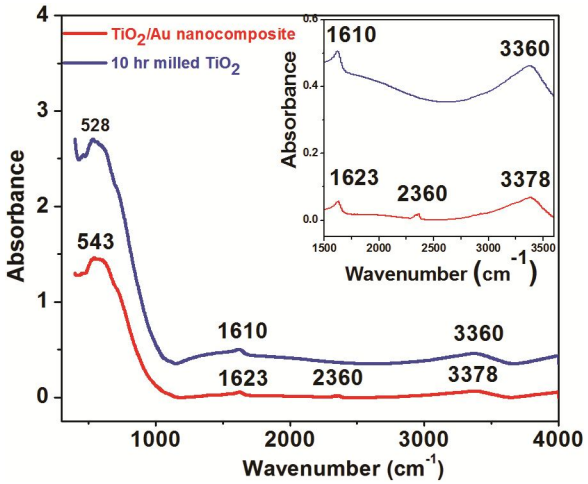


Fig. 6 – FTIR spectra of 10 h milled $TiO_2$ and $TiO_2$/Au nanocomposite. The inset shows the features in the region 1600-3600 $cm^{-1}$ for 10 h milled $TiO_2$ and $TiO_2$/Au nanocomposite.

$TiO_2$ semiconductor and thus accelerate their separation from photo-induced holes, leading to decrease in recombination rate of charge carriers[48].

The lower PL intensity in 10 h milled $TiO_2$ and $TiO_2$/Au nanocomposite indicates a delay in recombination rate and thus the photocatalytic activity of milled $TiO_2$ powder and $TiO_2$/Au nanocomposite is enhanced.

#### *3.2.3 FTIR studies*

The FTIR spectra of the milled $TiO_2$ and $TiO_2$/Au nanocomposite in 400 to 4000 $cm^{-1}$ region are shown in Fig. 6. The peaks at 1610 and 3360 $cm^{-1}$ in the spectra are assigned to the bending and stretching vibration, respectively, of the OH group on the surface of $TiO_2$[49,50]. In the spectrum of $TiO_2$, the peak at 528 $cm^{-1}$ (500 to 600 $cm^{-1}$), shows stretching vibrations of Ti-O peaks[51,52]. The peak at 2360 $cm^{-1}$ in the $TiO_2$/Au nanocomposite results from the adsorbed $H_2O$ molecules, which were not removed completely during the powder preparation technique. In $TiO_2$/Au nanocomposite, there is decrease in peak area and also shifting of peaks by 13 to 18$cm^{-1}$in comparison to 10 h milled $TiO_2$. This shifting of peaks is mainly due to the week interfacial interaction between the Au nanoparticles and $TiO_2$ powder[53].

## 4 Conclusions

Milling induces phase transformation in $TiO_2$from anatase to rutile through the intermediate srilankite phase. In addition, milling reduces the crystallite size of the powder. The adopted wet chemical synthesis technique facilitates the crystallization of amorphous phase of the milled powder to anatase phase. UV-Visible characterization indicates that Au reduces the band gap of the milled powder from 3.34 eV to 3.1 eV in the $TiO_2$/Au nanocomposite. $TiO_2$/Au nanocomposite exhibited a strong spectral response in the visible range (490 to 600 nm) due to the surface plasmon effect as well as light absorbance in the UV range. A weak interaction between Au and $TiO_2$ results small peak shift in the FTIR spectra. Au particles act as trap centres to inhibit the electron-hole recombination as a result the PL intensity in $TiO_2$/Au nanocomposite is decreased. The decrease in band gap and inhibition of electron-hole recombination in $TiO_2$/Au nanocomposite can increase its photocatalytic activities and hence this material could be used as a good candidate for photocatalysis.

## Acknowledgement

We thank Prof P K Sahoo, NISER, BBSR for providing SEM and PL characterization facilities.

## References

1 Zaleska A, *Recent Patents Eng*, 2 (2008) 157.
2 Diebold U, *Surf Sci Rep*, 48 (2003) 53.
3 Ma J, Ren W, Zhao J & Yang H, *J Alloys Compd*, 692 (2017) 1004.
4 4. Bai J & Zhou B, Chem Rev, 114 (2014) 10131.
5 Zalnezhad E, Hamouda A M S, Faraji G & Shamshirband S, *Ceram Int*, 41 (2015) 2785.
6 Smith S J, Stevens R, Liu S, Li G, Navrotsky A, Boerio-Goates J & Woodfield B F, *Am Mineralogist*, 94 (2009) 236.
7 Ghosh T B, Dhabal S & Datta A K, *J Appl Phys*, 94 (2003) 4577.
8 Muscat J, Swamy V & Harrison N M, *Phys Rev B*, 65 (2002) 224112.
9 Sen S, Ram M L, Roy S & Sarkar B K, *J Mater Res*, 14 (1999) 841.
10 Pan X, Chen Y, Ma X & Zhu L, *Trans Nonferrous Met Sci China*, 13 (2003) 271.
11 Liao S C, Chen Y J, Mayo W E & Kear B H, *Nanostruct Mater*, 11 (1999) 553.
12 Haines J & Léger J N, *Physica B*, 192 (1993) 233.
13 Rath H, Dash P, Som T, Satyam P V, Singh U P, Kulriya P K, Kanjilal D, Avasthi D K & Mishra N C, *J Appl Phys*, 105 (2009) 074311.
14 Mondal S, Madhuri R & Sharma P K, *J Alloys Compd*, 646 (2015) 565.
15 Gautam S K, Chettah A, Singh R G, Ojha S & Singh F, *Nucl Instrum Methods Phys Res B*, 379 (2016) 224.
16 Gribband A A & Banfield J F, *Am Mineralogist*, 82 (1997) 717.
17 Zhang H Z & Banfield J F, *J Mater Chem*, 8 (1998) 2073.
18 Chen M, He Y, Liu X, Zhu J & Liu R, *Powder Technol*, 311 ( 2017) 25.
19 19. Daniel M C & Astruc D, *Chem Rev*, 104 (2004) 293.
20 Her S, Jaffray D A & Allen C, *Adv Drug Delivery Rev*, 109 (2017) 84.

21 Notarianni M, Vernon K, Chou A, Aljada M, Liu J & Motta N, *Solar Energy*, 106 (2014) 23.
22 Fang C, Dharmarajan R, Megharaj M & Naidu R, *Trends Anal Chem*, 86 (2017) 143.
23 Piella J, Bastús N G & Puntes V, Chem Mater, 28 (2016) 1066.
24 Singh J, Sahu K, Pandey A, Kumar M & Mohapatra S, *Appl Surf Sci*, 411 (2017) 347.
25 Yin Y, Liu E, Li H, Wan J, Fan J, Hu X, Li J, Tang C & Pu C, *Ceram Int*, 42 (2016) 9387.
26 Sadrieyeh S & Malekfar R, *J Non-Cryst Solids*, 489 (2018) 33.
27 Debeila M A, Raphulu M C, Mokoena E, Avalos M, Petranovskii V, Coville N J & Scurrell M S, *Mater Sci Eng A*, 396 (2005) 61.
28 Tripathy B B, Sahoo P K, Mishra D K, Parashar S K S & Mishra N C, *Adv Sci Lett*, 20 (2014) 612.
29 Ren R, Rang Z & Shaw L L, *J Mater Sci*, 35 (2000) 6015.
30 Dutta H, Sahu P, Pradhan S K & De M, *Mater Chem Phys*, 77 (2002) 153.
31 Girot T, Devauxs X, Begin-Coling S, Caer G L & Mocellin A, *Philosophical Magazine A*, 81 (2001) 489.
32 Tripathy B B, Rath H, Mallick P & Mishra N C, *Adv Sci Eng Med*, 9 (2017) 144.
33 Yanagisawa I & Ovenstone J, *J Phys Chem B*, 103 (1999) 7781.
34 Wautelet M, Quenon P & Jadin A, *Semicond Sci Technol*, 3 (1988) 54.
35 Loganathan K, Bommusamy P, Muthaiahpillai P & Velayutham M, *Environ Eng Res*, 16 (2011) 81.
36 Mock J J, Barbic M, Smith D R, Schultz D A & Schultz S, *J Chem Phys*, 116 (2002) 6755.
37 Bian Z, Zhu J, Cao F, Lu Y & Li H, *Chem Commun*, 25 (2009) 3789.
38 Li X, Fan T, Zhou H, Zhu B, Ding J & Zhang D, *Microporous Mesoporous Mater*, 116 (2008) 478.
39 Haiss W, Thanh N T K, Aveyard J & Fernig D G, *Anal Chem*, 79 (2007) 4215.
40 Yang L, Li G H & Zhang L D, *Appl Phys Lett*, 76 (2000) 1537.
41 Serpone N, Lawless D & Khairutdinov R, *J Phys Chem*, 99 (1995) 16646.
42 Lei Y, Zhang L D, Meng G W, Li G H, Zhang X Y, Liang C H, Chen W & Wang S X, *Appl Phys Lett*, 78 (2001) 1125.
43 Choudhury B & Choudhury A, *J Lumin*, 136 (2013) 339.
44 Moon B K, Jeong J H, Yi S, Kim S C, Choi H & Kim J H, *Opt Mater*, 28 (2006) 676.
45 Liu B, Wen L & Zhao X, *Mater Chem Phys*, 106 (2007) 350.
46 Jagadale T C, Takale S P, Sonawane R S, Joshi H M, Patil S I, Kale B B & Ogale S B, *J Phys Chem C*, 112 (2008) 14595.
47 Zhou W, Liu H, Wang J, Liu D, Du G & Cui J, Appl Mater Interf, 2 (2010) 2385.
48 Jakob M, Levanon H & Kamat P V, *Nano Lett*, 3 (2003) 353.
49 Klingenberg B & Vannice M A, *Chem Mater*, 8 (1996) 2755.
50 Cerrato G, Marchese L & Morterra C, *Appl Surf Sci*, 70 (1993) 200.
51 Gao Y, Masuda Y, Peng Z, Yonezawa T & Koumoto K, *J Mater Chem*, 13 (2003) 608.
52 Shao G, Zhang X & Yuan Z, *Appl Catal B*, 82 (2008) 208.
53 Ryczkowski J, *Catalysis Today*, 68 (2001) 263.